Supplementary Information for

Instantaneous micropatterning of a double-network hydrogel surface triggered by mechanical force

Qifeng Mu[1], Kunpeng Cui[2], Zhijian Wang[1], Takahiro Matsuda[3], Wei Cui[3], Hinako Kato[1], Shotaro Namiki[1], Tomoko Yamazaki[1], Martin Frauenlob[1], Daniel R. King[3], Takayuki Nonoyama[3], Masumi Tsuda[2,4], Shinya Tanaka[2,4], Tasuku Nakajima[2,3]*, Jian Ping Gong[2,3]*

[1]Graduate School of Life Science, Hokkaido University, N21W11, Kita-ku, Sapporo 001-0021, Japan;
[2]Institute for Chemical Reaction Design and Discovery (WPI-ICReDD), Hokkaido University, N21W10, Kita-ku, Sapporo 001-0021, Japan;
[3]Faculty of Advanced Life Science, Hokkaido University, N21W11, Kita-ku, Sapporo 001-0021, Japan;
[4]Department of Cancer Pathology, Faculty of Medicine, Hokkaido University, N15, W7, Kita-ku, Sapporo 060-8638, Japan
*E-mail: tasuku@sci.hokudai.ac.jp; gong@sci.hokudai.ac.jp

This PDF file includes:
Materials and Methods
Supplementary Text
Fig. S1 to S31
Table S1
References

Table of Contents

Materials

Water (H_2O) used was purified by a lab water purification system (Merck KGaA, Darmstadt, Germany). Acrylamide (AAm) was purchased from Junsei Chemical, 2-Acrylamido-2-methylpropanesulfonic acid sodium salt (NaAMPS) (49.7 wt% aqueous solution) was provided by Toa Gosei. *N,N′*-Methylenebisacrylamide (MBA), 2-oxoglutaric acid (α-keto), *N*-isopropylacrylamide (NIPAm), acrylic acid (AAc), sodium *p*-styrenesulfonate (NaSS), and 3-(methacryloylamino)propyltrimethylammonium chloride (MPTC) were purchased from Fujifilm Wako Pure Chemical Corporation. 8-Anilino-1-naphthalenesulfonic acid (ANS) was purchased from Tokyo Chemical Industry. Deuterium oxide (D_2O), sodium hydroxide (NaOH), and hydrochloric acid (HCl) were purchased from Fujifilm Wako Pure Chemical Corporation. All the chemicals were used as received.

Characterization of hydrogels

Hydrogel surface elastic modulus. A sphere metal indenter (radius: ~0.25 mm) was applied to probe the local surface elastic modulus of different hydrogels at a constant rate of 1 mm min^{-1} under water. The sphere metal indenter was rigid, frictionless, and impermeable. Firstly, as-prepared different hydrogels were cut into fixed square shape (size: 2 cm×2 cm, thickness: 3.5–5 mm) then immersed in pure water to equilibrium state prior to the indentation measurement. The surface elastic modulus measurements were carried out in a water bath to prevent water evaporation[1,2]. The square samples were fixed on a rigid plate in a home-made box, where the rigid plate was a frictionless, impermeable metal substrate. According to the Hertzian contact theory, surface elastic modulus *E* (Pa), a parameter that characterizes stiffness of a material, is expressed by the following equation[3,4]

$$E = \frac{3}{4} l^{-\frac{3}{2}} f R^{-\frac{1}{2}} (1 - v_P^2) \quad (1)$$

where *l* is depth, *f* is indentation force, *R* is the radius of sphere indenter, and v_p is Poisson's ratio and set to be 0.5. Therefore, the surface elastic modulus was calculated from the initial slope (indentation depth: 0-0.01 mm) of the f-$l^{3/2}$ indentation curves. The calculated surface modulus was the average value of five replicates, which was summarized in Table S1.

We prepared the DN hydrogel surfaces using a surface-bulk transition

technique[2], and tough hydrogel surfaces with the first rigid networks (densely crosslinked polymer network strands) were confirmed by the surface elastic modulus measurements, as shown in Fig. S3b.

Attenuated total reflectance Fourier-transform infrared (ATR FT-IR) spectroscopy measurement. The hydrogel surface layer chemical signal was probed by an ATR FT-IR spectroscopy (FT-IR 6600 spectrometer, JASCO, Japan). With its shallow detection range (1–2 μm) and high resolution in wavenumber (~2 cm^{-1}), the ATR FT-IR measurements focused on the chemical group at the interface between the hydrogel and its immediate surroundings. We confirmed that the first brittle network PNaAMPS is on the DN hydrogel surfaces based on the stretching vibration peak (1042 cm^{-1}) of sulfonic group from PNaAMPS chains[2]. The as-prepared DN and SN hydrogels were immersed in pure water for at least one week to equilibrium swelling then immersed in D_2O for two days prior to the measurements. The wavenumber region was 1800–800 cm^{-1}, number of scans was 64, resolution was 2 cm^{-1}. The infrared spectra and linear polymer structure with functional groups were shown in Fig. S2. Infrared absorption peak at 1042 cm^{-1} indicated that there is first network on the tough DN hydrogel surfaces prepared by our surface-bulk transition technology.

Tensile and fracture measurements. The mechanical tensile measurements were performed using a commercial tensile-compressive tester (Tensilon RTC-1310A, Orientec Co., Ltd.) at a displacement velocity of 100 mm min^{-1} in air (25 ^oC). Hydrogels were cut into dumbbell-shaped samples with the standard JIS-K6251-7 size (12 mm length × 2 mm width × 1.5 mm thickness). The tensile test (or uniaxial stretching) was applied to characterize mechanical properties of hydrogels, fracture stress, fracture strain, and work of extension[5].

The fracture measurements were performed to characterize hydrogel toughness (fracture energy or tearing energy) in air by using the same commercial tester mentioned above. In the fracture measurements, the samples of 1.5 mm (t_0) in thickness were cut into trousers-like shape with cut length c based on the standard JIS-K6252 1/2 sizes (50 mm length × 7.5 mm width (h_0), the cut length (or initial notch length) c was 20 mm using a cutting machine (Dumb Bell Co., Ltd.). One leg of the trouser-shaped DN hydrogel was fixed and the other leg was pulled away at a velocity of 100 mm min^{-1}. The

tearing energy Γ was calculated using the following equation[6,7].

$$\Gamma = \frac{2\lambda f}{t_0} - W \cdot h_0 \approx \frac{2f}{t_0} \quad (2)$$

where f and W is the tearing force and the arm's stored elastic energy per unit volume during crack propagation. When the arm's stretch is small, the fracture energy is approximated as $\Gamma \approx 2f/t_0$. From these tests, mechanical properties of the DN hydrogel were confirmed: fracture stress 0.96±0.06 MPa, fracture strain 10.66±1.67, work of extension 8.23±1.56 MJ m^{-3}, and toughness 2.91±0.25 kJ m^{-2}.

Cylindrical indentation measurements. The indentation measurements were carried out using an MCT-2150 mechanical tester (A&D Co., Ltd.) in a glove box at 25 °C for the DN hydrogel with NIPAm (Fig. 2a, 2d), and using a Shimadzu Autograph AG-X 10N tensile machine in air at 25 °C for the DN hydrogel without monomers (Fig. S7-S9). To characterize the mechanical properties of tough DN hydrogel surfaces with and without feeding monomers, a cylindrical steel indenter with smooth cutting edge (diameter: ~568 μm) was fixed on load cell by screw, the hydrogels were cut into disc shape (diameter: ~15 mm) then glued to a rigid glass plate from Matsunami company of Japan (S2112) prior to the surface indentation. The indentation velocity was 10 mm min^{-1} in the glove box and 1 mm min^{-1} in air.

Surface observation of different hydrogel surfaces and steel indenters by a three-dimensional (3D) laser microscope. Different swollen hydrogel surfaces were observed in air by a 3D laser microscope (VK-9710, Keyence Co., Ltd.). Free water on hydrogel surfaces was wiped out by clean tissues prior to observation. The magnification was ×10, and the resolution was 0.5 μm for each observation. Surface roughness value R_a was calculated by selecting a small square area (500 μm × 500 μm) on hydrogel surfaces. Side and top surfaces of steel indenters were also observed by the laser microscope, as shown in Fig. S10. Different hydrogel surfaces, microstructures, patterns, and the reswollen zones were also observed by the microscope, profile and size of microstructures were measured by a software VK Analyzer, as shown in Fig. S4, Fig. S6, Fig. S7c, Fig. S10-12, Fig. S16, Fig. S18a, Fig. S19 a, Fig. S21a, Fig. S22a, and Fig. S25.

Monomer conversion ratio in force-triggered radical polymerization

In-situ transmission Fourier-transform near-infrared (FT-NIR) spectroscopy measurement. The conversion ratio is an indicator of monomer reactivity in radical polymerization. To quantify different monomers conversion ratio in the course of force-triggered radical polymerization, an in-situ transmission FT-NIR spectroscopy was used. The near-infrared spectroscopy is sensitive to overtones and combinations of vibrations[8]. There was a characteristic absorption peak at approximately 1613–1639 nm (wavenumber is 6200–6100 cm^{-1}, within the near-infrared region) corresponds to C–H overtone stretching at the C=C double bond of alkene monomers. We performed the measurements in a customized small glove box filled with argon, DN hydrogels fed with different monomers were stretched to a tensile strain (ε ~3) by a set of home-made clamps, the strain rate was ~1 s^{-1} and it took approximately ~6 s in the loading-unloading process, the tensile stress was around ~0.9 MPa. The absorbance *A* was divided by sample thickness *l*, i.e., the normalized absorbance *A/l.* The normalized absorbance was analysed by the Beer-Lambert law[9], which was normally combined in the following mathematical equation.

$$A = \log_{10}\left(\frac{I_o}{I}\right) = \epsilon l c \tag{3}$$

$$A/l \propto c \tag{4}$$

where ϵ is the molar absorption coefficient ($M^{-1}cm^{-1}$), *c* is the molar concentration of the attenuating substances (M), I_o is the intensity of incident infrared light, and *I* is the intensity of transmitted infrared light. Note that ϵ is a characteristic constant related to the substances, so the value of *A/l* is proportional to the molar concentration of substances.

The normalized absorbance *A/l* is proportional to monomer concentration *c* based on the Beer-Lambert law. The measurement background was the DN hydrogel without monomers, the baseline of water and polymer networks was subtracted in this experimental section. We firstly confirmed the transmission near-infrared spectrum calibration curves of DN hydrogels fed with different monomers (monomer concentration from 0 M to 1.0 M) prior to the monomer conversion ratio measurements. A linear correlation between the normalized absorbance peak area S and the monomer concentration c was observed for DN hydrogels fed with different monomers (Fig. S13). The observed normalized

absorption peak area S (selected peak area region within 6250–6100 cm^{-1}, unit/cm) depended on the monomer concentration.

$$S = \alpha c \tag{5}$$

Where α is the proportional constant which slightly depends on the monomer species (α is 9.14, 9.30, 11.95, and 10.38 for the monomers NIPAm, AAc, NaSS, and MPTC, respectively).

We measured the change of monomer concentration in tough DN hydrogel bulks before stretching and after stretching using the in-situ FT-NIR. The force-triggered variation in monomer concentration was associated with a change in transmitted light intensity at the monomer peak position around 6200–6100 cm^{-1}.

Here, the sample thickness l was the initial thickness of DN hydrogels with monomers before stretching, under an assumption that thickness change by stretching is negligibly small. Since the normalized absorption peak area S of different monomers is proportional to monomer concentration, the monomer conversion ratio (Conv) can be calculated based on the equation.

$$\begin{aligned} \mathrm{Conv} &= (1 - c_\mathrm{t}/c_\mathrm{o}) \\ &= (1 - S_1/S_0) \end{aligned} \tag{6}$$

Here, c_t and c_0 is the monomer concentration at time t, and initial monomer concentration, respectively. S_1 and S_0 is the normalized absorption peak area of the monomers at time t and the initial time. The conversion ratio of monomer NIPAm was around 0.7 in the force-triggered radical polymerization at 1 min after the stretch. Then we measured the transmission near-infrared spectrum change for different monomers (initial concentration was 1.0 M) when the radical polymerization time was fixed at 1 min, as shown in Fig. S14. Monomer conversion ratios for different monomers (NaAMPS, NIPAm, AAc, NaSS, and MPTC) were 0.802 ± 0.005, 0.692 ± 0.007, 0.498 ± 0.016, 0.459 ± 0.008, and 0.593 ± 0.025, respectively. Error ranges represent standard deviation from three replicates. The measurement parameters for in-situ transmission FT-NIR were constant in the experiment. The number of scans was 32 that took around 20 s (hence the measured values at 1 min are the average of approximately 60-80 s after the stretching), resolution was 2 cm^{-1}, detector was triglycine sulfate (TGS), region of the spectral scan was 6300-6000 cm^{-1}, sample thickness was around ~2.5 mm.

Kinetics of force-triggered radical polymerization

Time-resolved near-infrared spectroscopy measurements. To study the kinetics of force-triggered radical polymerization with different monomers, a time-resolved near-infrared spectroscopy was used. The rapid scan system of the spectroscopy enables the instrument to measure the spectrum every 0.07–0.08 second (one scan per one data) for providing real-time analysis of reaction kinetics. The DN hydrogels with different monomers (NaAMPS and NIPAm, initial concentration was 1.0 M without crosslinker) were stretched to a tensile strain ($\varepsilon \sim 3$) in a customized small glove box filled with argon, the strain rate was ~3 s^{-1} and it took approximately ~1 s in the loading process, the tensile stress was around ~0.9 MPa, the thickness of DN hydrogels with different monomers was 1.5–2 mm. We measured the absorption value change for only one wavenumber (6175 cm^{-1}) in the time-resolved test. Monomer concentration decay during the polymerization was detected by the near-infrared spectroscopy at 298 K (25 ^{o}C) (Fig. S20), which was fast and efficient (within tens of seconds) in our force-triggered radical polymerization system. For smoothing the data, we took the moving average of the absorbance with a width of ± 0.3 s.

Programmable complex micropatterning of DN hydrogel surfaces

Preparation of indenters by three-dimensional (3D) printing. The complex patterned indenters were printed using a commercial high-precision 3D printer system (Agilista 3100, Keyence Co., Ltd.). The surface patterns of indenters were designed by a commercial software Solidworks (Dassault Systèmes SolidWorks Corporation, USA) prior to the course of 3D printing. The surface quality of 3D printed indenter was defined as glossy surface. The material of 3D printed indenters was high strength resin. The topographic height of patterns was ~2 mm. The photos of 3D printed indenters are shown in Fig. S23.

Creating complex patterns by indentation. Firstly, the 3D printed indenters were fixed on a home-made metal holder, and the holder with indenters was fixed on the sensor of a small tensile machine (MCT-2150, A&D Co., Ltd.) using a screw. The selectively mechanical indentation was performed in a glove box, as shown in Fig. S24a. The DN hydrogels were immersed in NIPAm-ANS

aqueous solution (NIPAm: 1.0 M, ANS: 0.3 mM) for overnight. The immersed DN hydrogels were fixed on a rigid glass plate by glue, then were moved to an argon glove box to remove oxygen. The complex patterns were created by indenting selectively on DN hydrogel surfaces under the solution using the 3D printed indenters (Fig. S23). The indentation depth was around 1 mm for these complex patterns. After the indentation, the DN hydrogels with patterns were immediately observed at high temperature (50 ^{o}C) and ultraviolet light (UV) irradiation.

Specific applications of DN hydrogels with micropatterns

Contact angle measurements of the patterned hydrogel surfaces. Liquid contact angle of the patterned hydrogels was measured by using a Drop master 300 (Kyowa Interface Science Co., Ltd.) in air at 25 ^{o}C. For the static contact angle measurements, liquid volume was 10 μL for water droplet (deionized water), free water on hydrogel surfaces was wiped off using cleaning tissues prior to each measurement, waiting time was 5 s for each measurement (Fig. S27-S29). The dynamic contact angle measurements were also carried out using the same machine, liquid droplet (10 μL) was extruded with a pipette (Fig.S30). The contact angle was the average value of three measurements. The dependence of water transport velocity on water volume for different patterned DN hydrogel surfaces is shown in Fig.S31.

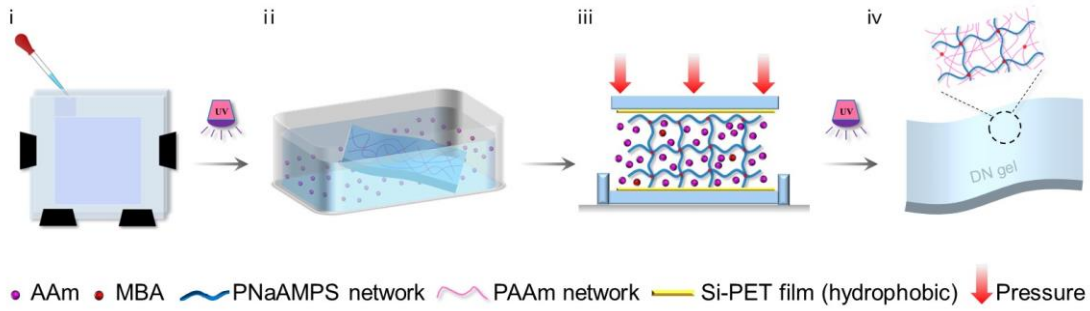

Fig. S1. Schematic illustration of fabrication of tough double-network (DN) hydrogels with the double-network structure to the top-most surface layer. i. The first network hydrogel was polymerized in a glass mould under UV light. ii. The prepared first network hydrogel was immersed in the AAm monomer aqueous solution. iii. A hydrophobic silicone-coated PET (Si-PET) film was covered on the glass mould surface by pressure (~0.8 kPa) during the second network synthesis to completely remove surface solution (residual AAm monomer aqueous solution), which also prevented the formation of the electric double layer at PNaAMPS-glass interface. Through this method, contact of PNaAMPS hydrogel with the hydrophobic surface of the Si-PET film was ensured.

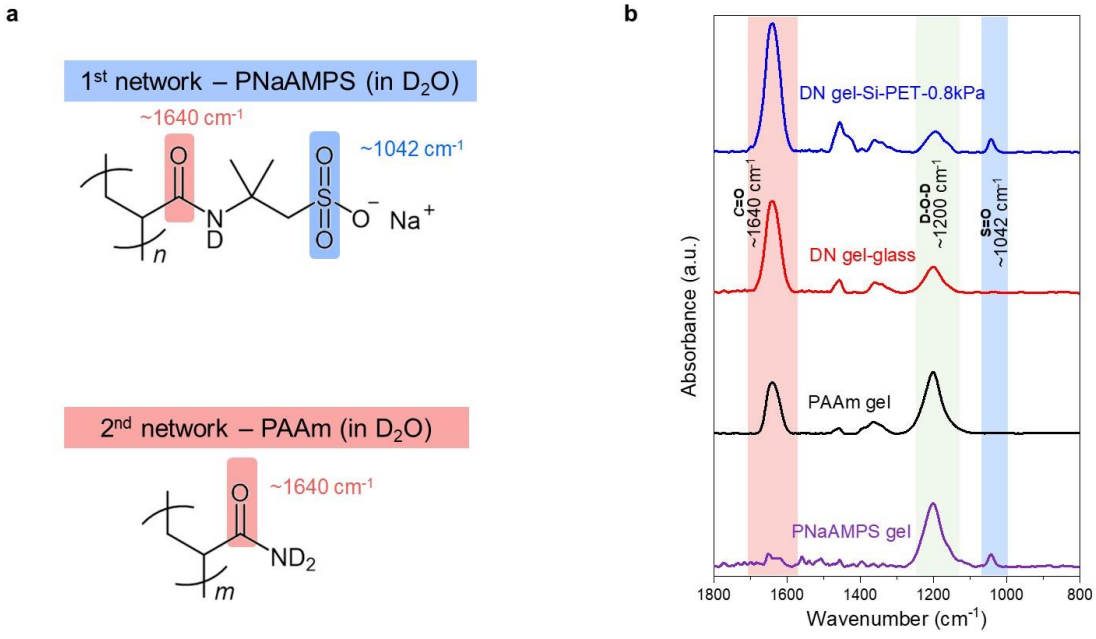

Fig. S2. a. Polymer network structures with functional groups. **b**. DN hydrogels with its second network prepared on the Si-PET film covered glass mould (coded DN gel-Si-PET-0.8kPa) show the obvious PNaAMPS signal at ~1042 cm^{-1}, while DN hydrogels with its second network prepared on glass mould (coded DN gel-glass) do not. These results indicate that the DN hydrogel structure is formed even at the top-most surface in the former DN hydrogels while the surface of the latter DN hydrogels is covered by PAAm.

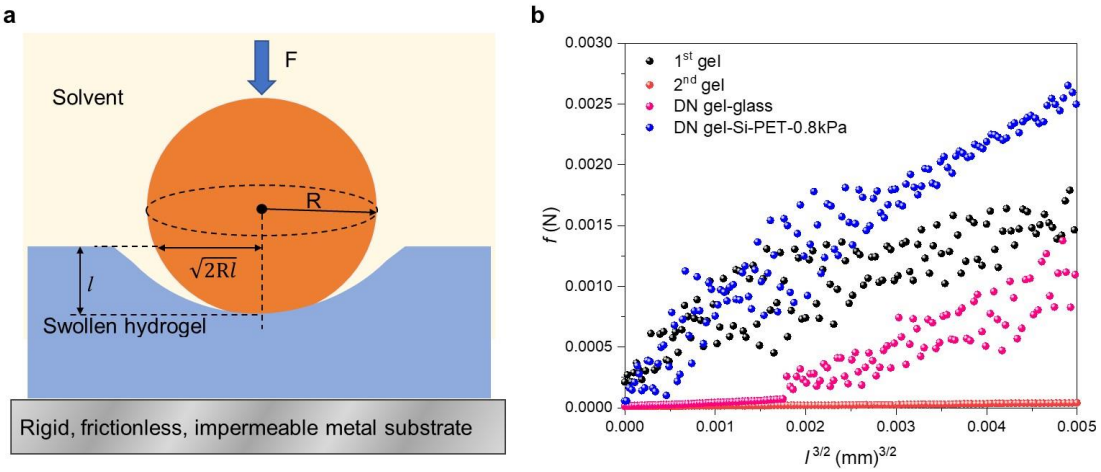

Fig. S3. a. Schematic illustration for hydrogel surface indentation measurements under water using a sphere metal indenter. Hydrogel thickness was 3.5–5 mm, which was far larger than the indentation depth (~0.029 mm) in the experiments. **b.** Indentation curves of f-$l^{3/2}$ for different indentation measurements, the slopes of curves are proportional to the surface elastic moduli of different hydrogels. DN hydrogels with its second network prepared on Si-PET film covered glass mould show the almost same modulus as the single first network, while DN hydrogels with its second network prepared on glass mould show a lower modulus than the single first network. These results again indicate that the double-network structure is formed even at the top-most surface in the former DN hydrogels while the surface layer of the latter DN hydrogel is covered by the soft second network. These results are consistent with the IR results shown in Fig. S2.

Table S1. Surface elastic modulus of the different hydrogels (1st gel is PNaAMPS SN gel,1-4-1), 2nd gel is PAAm SN gel (2-0.01-0.01), DN gel-glass and DN gel-Si-PET-0.8kPa are DN gels with different surfaces (1-4-1, 2-0.01-0.01).

Hydrogels	1st gel	2nd gel	DN gel-glass	DN gel-Si-PET-0.8kPa
Surface elastic modulus (kPa)	661.2 ± 88.9	6.6 ± 0.1	14.2 ± 0.3	683.2 ± 52.9

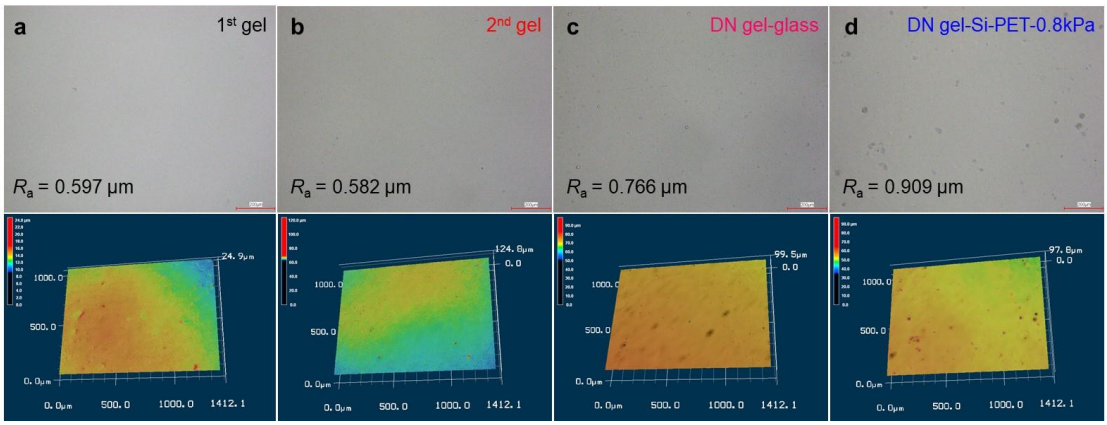

Fig. S4. Surface topography (roughness) of different hydrogels observed by 3D laser microscope in air. Here, R_a was calculated as the roughness average of gel surfaces measured microscopic peaks and valleys. **a**. 1st gel (PNaAMPS SN gel), **b**. 2nd gel (PAAm SN gel), **c**. DN gel-glass (DN gel prepared between glasses), **d**. DN gel-Si-PET-0.8kPa (the second network of DN gel was prepared between silicon-coated PET film under the pressure of ~0.8 kPa). Scale bar, 200 μm.

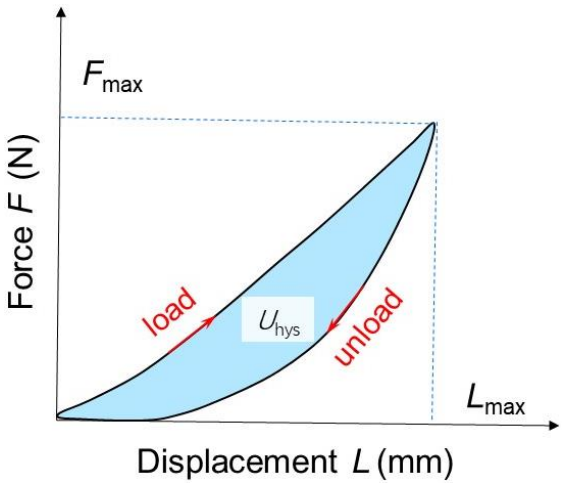

Fig. S5. Quantification of the mechanical energy dissipated by cyclic indentation on tough DN hydrogel surfaces using a cylindrical steel indenter. The area beneath the force-displacement curve gives the work done by mechanical force to the DN hydrogel surfaces.

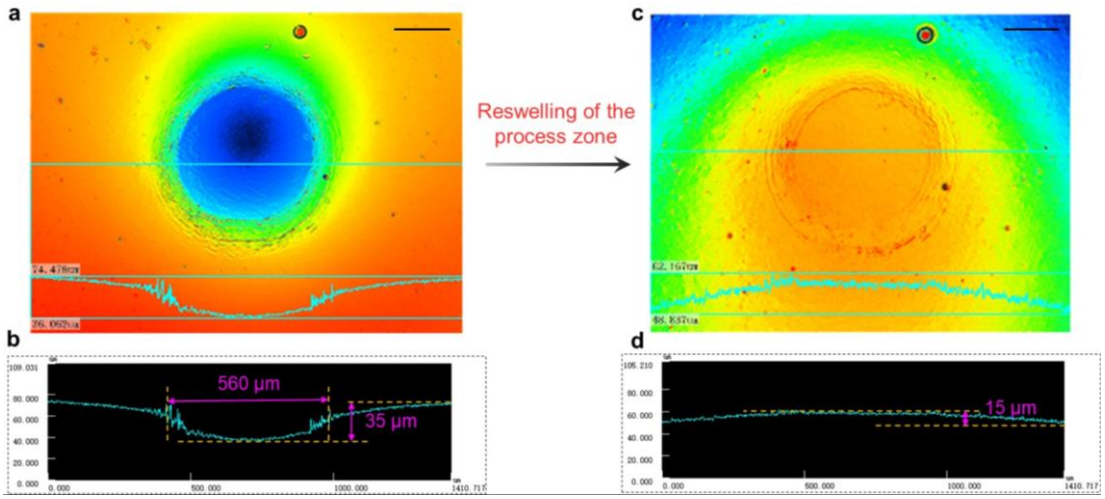

Fig. S6. Reswelling of the process zone (or damaged zone) on DN hydrogel surfaces. Immersion time in water for the reswelling was several seconds. **a**. Image of the process zone on DN hydrogel surface. **b**. Profile and size of the process zone. **c**. Image of the reswollen zone on DN hydrogel surface**. d**. Profile and height of the reswollen zone. Scale bar, 200 μm. A cylindrical steel indenter of diameter d = 568 μm and displacement L_{max} = 1000 μm, DN hydrogel thickness was ~3.8 mm.

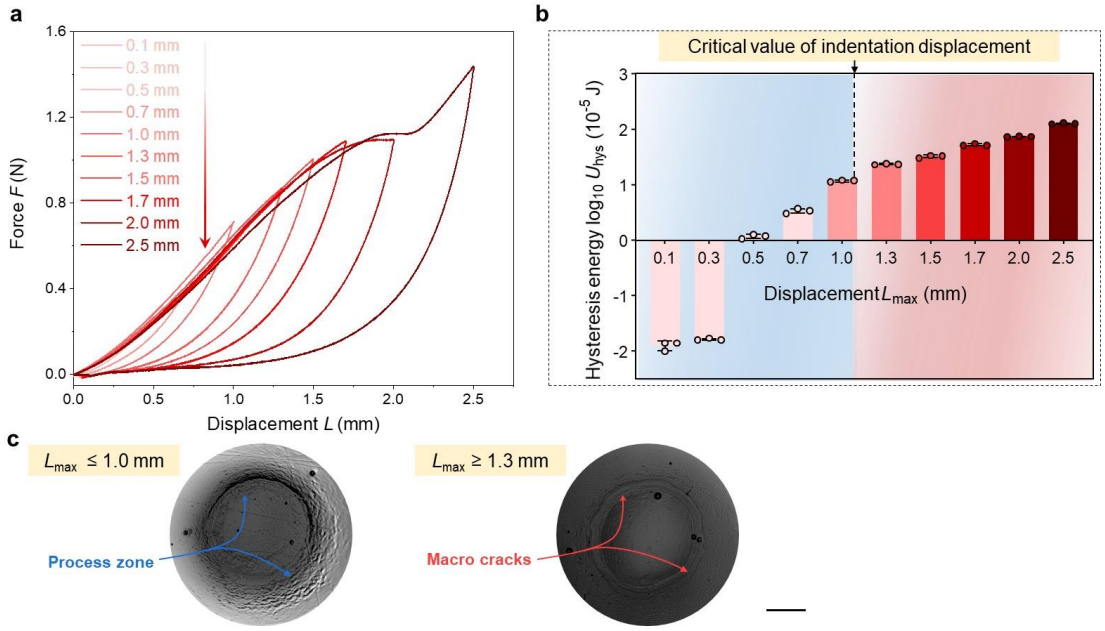

Fig. S7. Mechanical indentation on the DN hydrogel surfaces with different displacements L_{max} using a cylindrical steel indenter, DN hydrogel thickness was ~3.8 mm. **a**. Pronounced hysteresis for the different mechanical indentation displacements. **b**. Calculated hysteresis energy for different indentation displacements. **c**. Microscope images of the process zones on DN hydrogel surfaces. When displacement L_{max} was increased beyond 1.0 mm, macro cracks appeared on DN hydrogel surfaces, which was marked by the arrow. Accordingly, the maximum displacement of intender without macroscopic damage was 1.0 mm. The displacement velocity was 1 mm min^{-1}. Error bars represent standard deviation from three replicates. Scale bar, 200 μm.

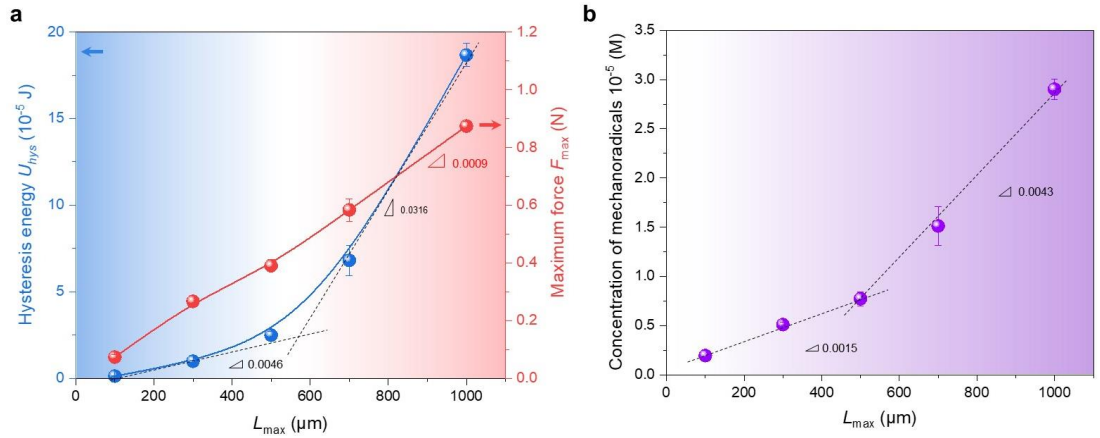

Fig. S8. a. The hysteresis energy U_{hys} and maximum force F_{max} measured at various indentation displacements L_{max} by mechanical indentation without monomer supply in the air (a cylindrical steel indenter diameter was d = 568 μm, the velocity of indentation was 1 mm min^{-1}, DN hydrogel thickness was ~3.8 mm). The U_{hys} was estimated from $U_{\mathrm{hys}} = \int_0^{L_{max}} (F_{\mathrm{load}} - F_{\mathrm{unload}})\mathrm{d}L$, which was indicated in Fig. S5. **b**. The concentration of mechanoradicals in the process zone changed with indentation displacement L_{max}. The dissipated energy per mole of strands of the first network was estimated based on the analysis by Lake and Thomas[10]. Here, the mechanical energy required to break one C-C covalent bond, ΔU_{act}, was considered to be 25% of the C-C bond dissociation energy E_b (~350 kJ/mol). The number of C-C bonds in the bridging strands of the first network, N, was estimated by using the affine network theory[11]. Here, N for the first network in the current study (synthesized from 1.0 M NaAMPS and 40 mM MBA) was estimated to be ~580 according to our previous work[12,13]. The process zone volume was assumed as $\pi(d/2)^2 L_{max}$. For example, when L_{max} was 1000 μm, the volume of process zone was π(568 μm/2)^2 ×1000 μm = 2.53×10^{-7} dm^3, and the hysteresis energy U_{hys} was 1.87×10^{-4} J. The mechanical energy U required to break a polymer strand with N monomers was estimated as $U = N\Delta U_{act} \approx$ 580 × (350 kJ mol^{-1} × 0.25) = 5.1×10^7 J mol^{-1}. The number of moles of mechanoradical was $2(U_{hys}/U)$ = 7.4×10^{-12} mol, and the mechanoradical concentration was roughly estimated as (7.4×10^{-12} mol)/(2.5×10^{-7} dm^3) =2.9×10^{-5} mol dm^{-3} or 2.9×10^{-5} M.

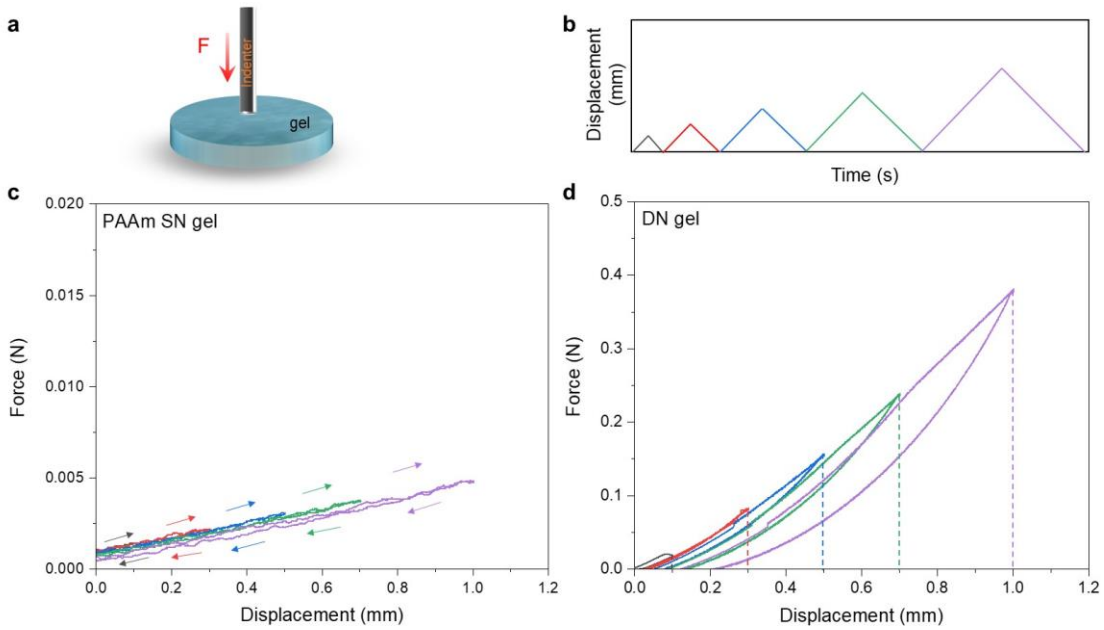

Fig. S9. Cyclic indentation on hydrogels using a cylindrical steel indenter (diameter d = 568 μm) in air. **a**. Schematic illustration for the cyclic indentation. **b**. Applied displacement changes over time for the cyclic indentation. **c**. Force-displacement curves show that PAAm SN gel surface is nearly elastic, PAAm gel thickness was ~5 mm. **d**. Displacement-force curves show that DN hydrogel surface is a tough surface with pronounced hysteresis, gel thickness was ~3.8 mm. Displacement velocity was 1 mm min^{-1}.

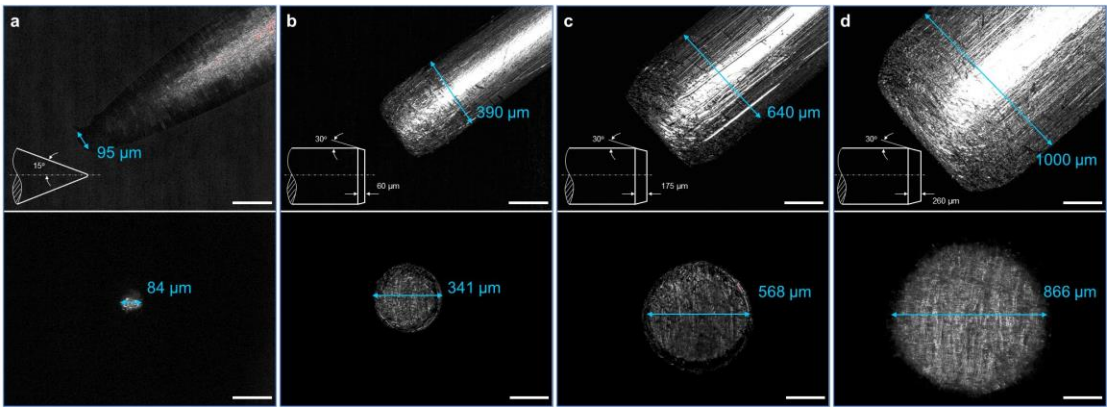

Fig. S10. a-d, Microscope images of the cylindrical steel indenters with different diameters. Scale bar, 200 μm.

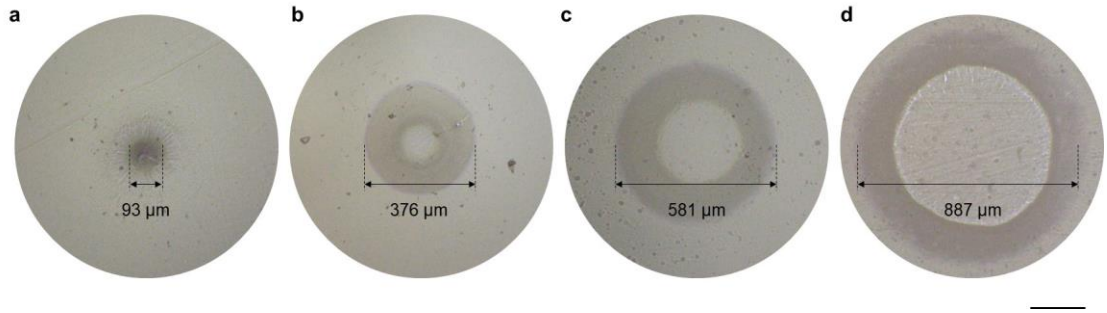

Fig. S11. a-d. Microscope images of the microstructures on DN hydrogel surfaces, which were indented with different cylindrical steel diameters (see Fig. S10). The scale and shape of microstructures depends on the indenters. The experiments were carried out in NIPAm aqueous solution (NIPAm: 1.0 M) under argon atmosphere. The indenter diameters were 84, 341, 568, and 866 μm for a, b, c, and d, respectively. The indentation depth L_{max} was 1000 μm. Scale bar, 200 μm.

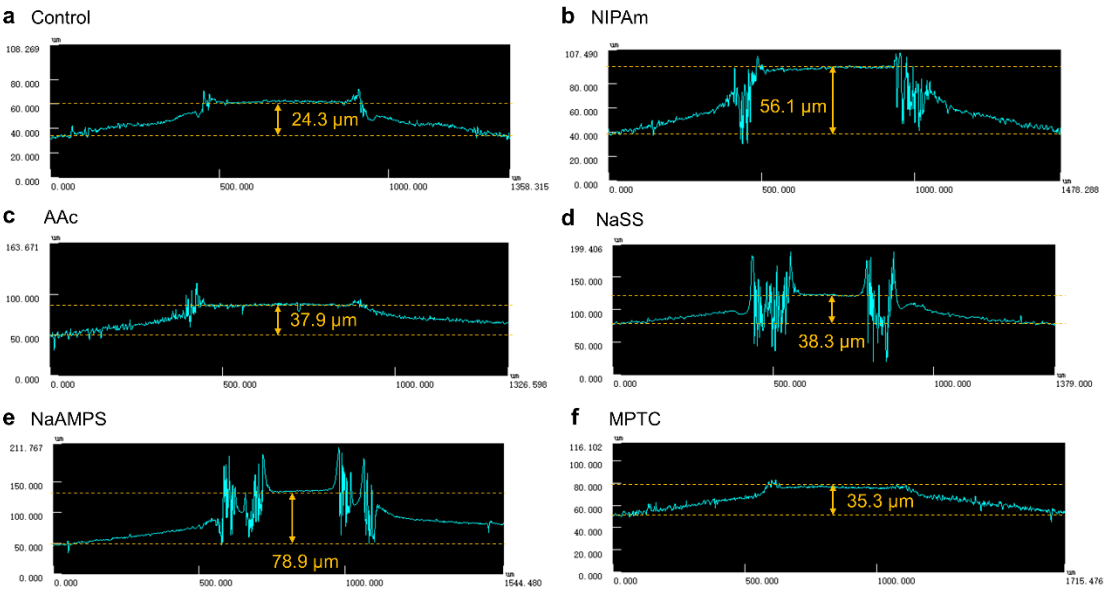

Fig. S12. The typical profiles of the microstructures on DN hydrogel surfaces using different functional monomers, the control sample was prepared without monomer and crosslinker supply. Monomer concentration was 1.0 M without crosslinker for all cases except for the control.

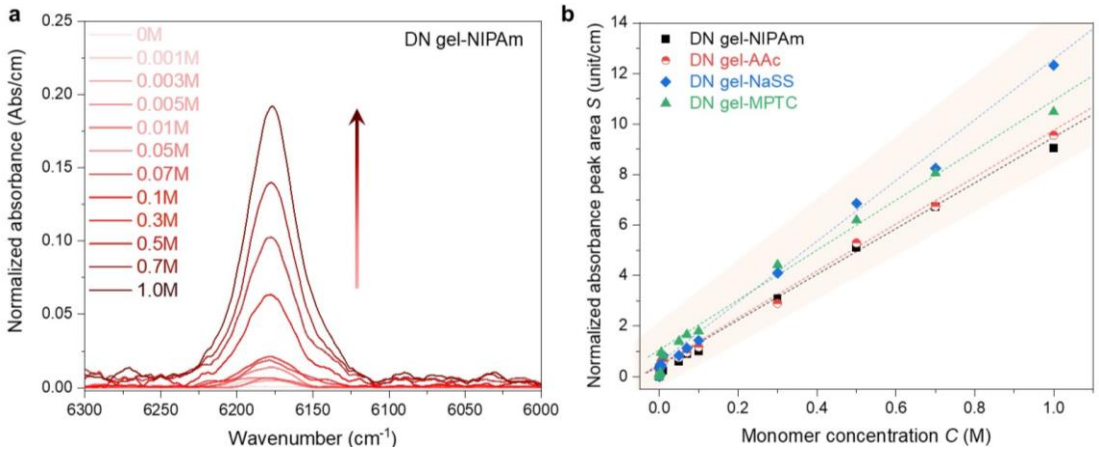

Fig. S13. **a**. Transmission near-infrared spectrum of DN hydrogels fed with different monomer concentrations (NIPAm, 0 M-1.0 M). **b**. Calibration curves of DN hydrogels fed with different monomers.

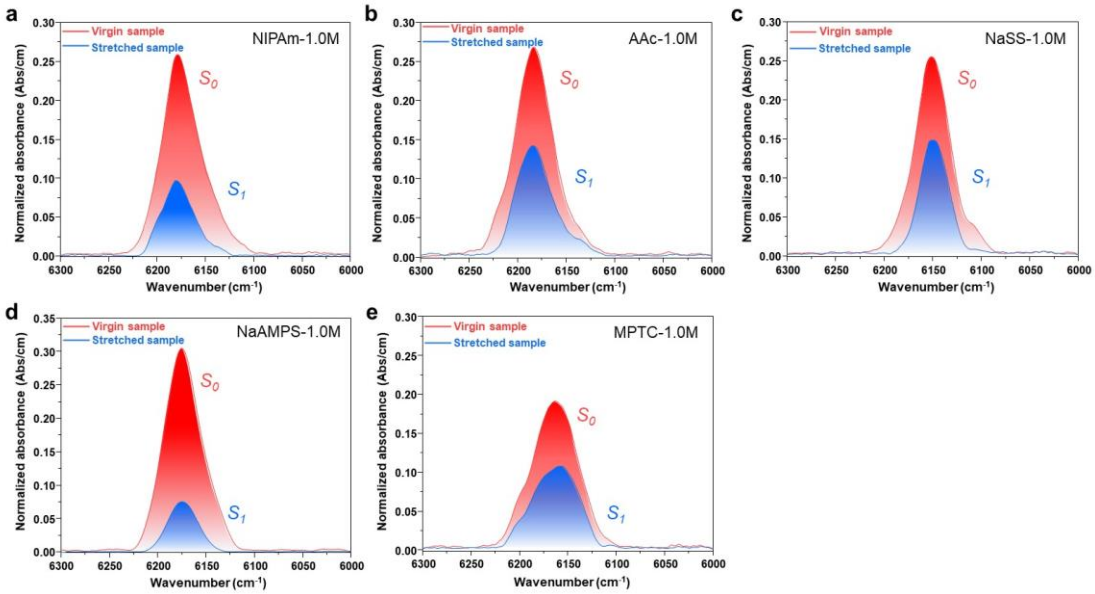

Fig. S14. Transmission near-infrared spectra of DN hydrogel fed with different monomers before stretching (S_0) and after stretching (S_1), measurement waiting time was 1 min. **a**. NIPAm-1.0M (initial concentration was 1.0 M), **b**. AAc-1.0M, **c**. NaSS-1.0M, **d**. NaAMPS-1.0M, **e**. MPTC-1.0M. Crosslinker (MBA) was not fed in this experiment.

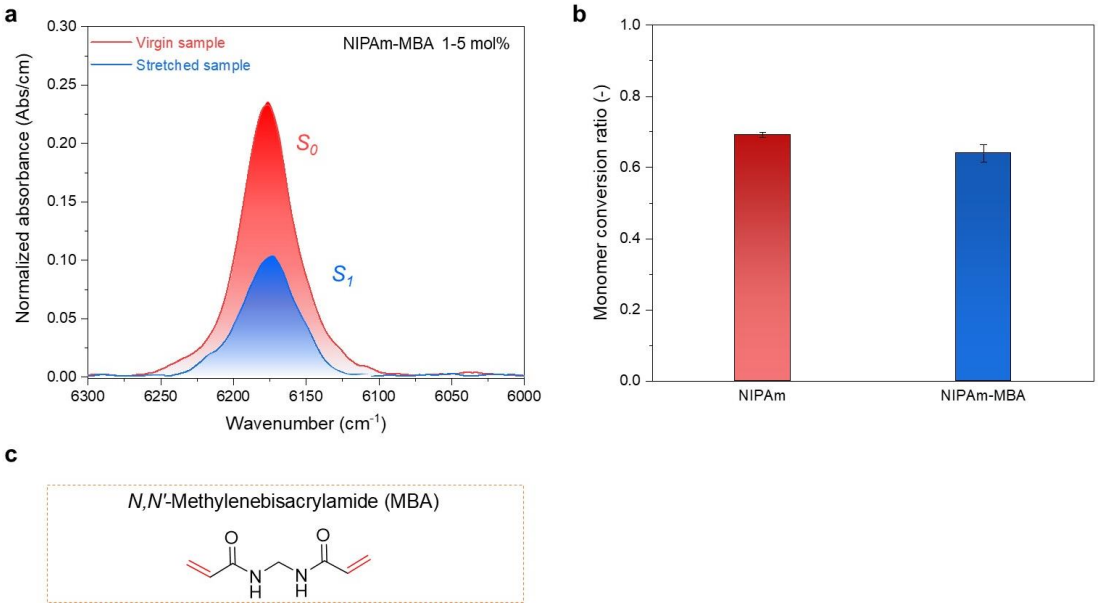

Fig. S15. a. Transmission near-infrared spectra of DN hydrogel fed with NIPAm-MBA 1-5 mol% before stretching (S_0) and after stretching (S_1), measurement waiting time was 1 min. **b**. The comparison of conversion ratio for DN hydrogels fed with NIPAm and with NIPAm-MBA (1-5 mol%, NIPAm monomer concentration was 1.0 M, the molar ratio of crosslinker MBA respect to NIPAm monomer was 5 mol%). **c**. Molecular structure of *N,N'*-methylenebisacrylamide (MBA).

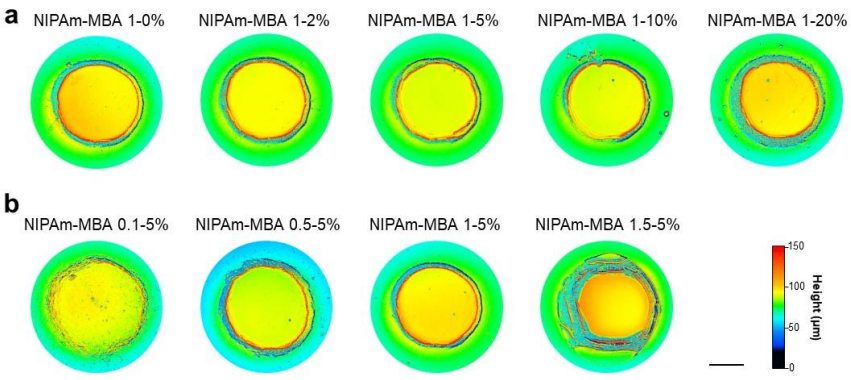

Fig. S16. a. Three-dimensional laser microscopy observation of the microstructures using different crosslinker concentrations (sample NIPAm-MBA 1-0% indicates that the monomer NIPAm concentration was 1.0 M and crosslinker MBA concentration was 0 M). **b**. Three-dimensional laser microscopy observation of the microstructures using different monomer concentrations. Scale bar, 200 μm.

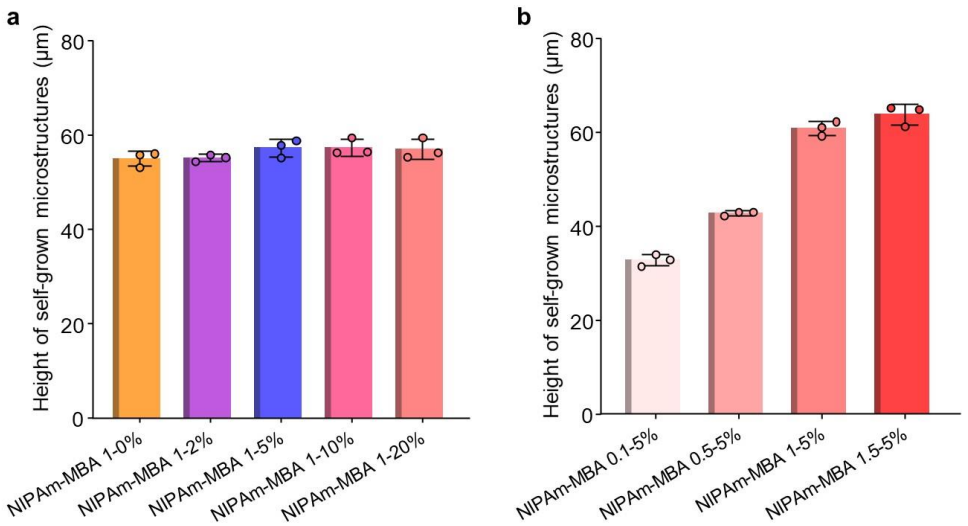

Fig. S17. a. The height of microstructures using different crosslinker ratios (here, the percentage was molar percentage). **b**. The height of microstructures using different monomer concentrations.

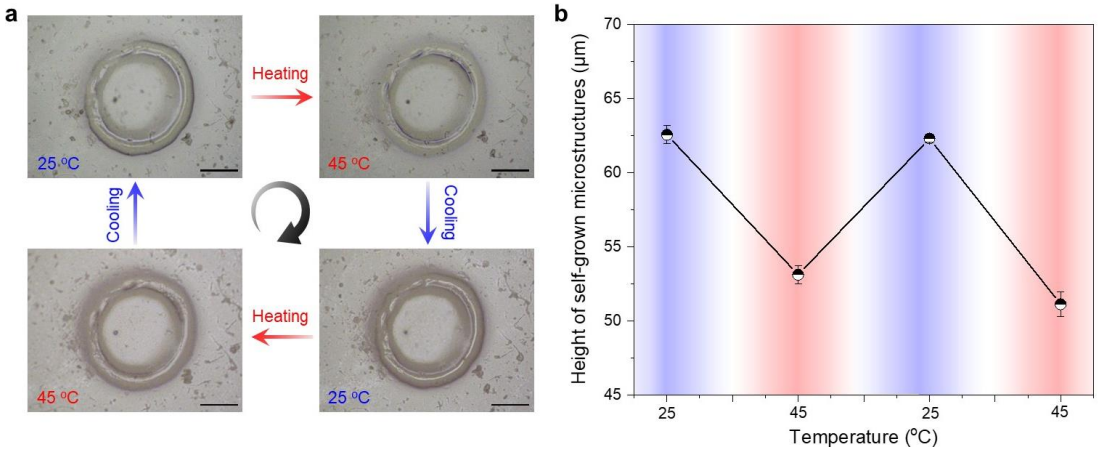

Fig. S18. Thermo-responsive microstructures using NIPAm (1.0 M, without crosslinker). **a**. Microscope images of the microstructures at different temperatures (with water in air). Scale bar, 200 μm. **b**. Height of microstructures changed with temperature cycle. Error bars represent standard deviation from three replicates.

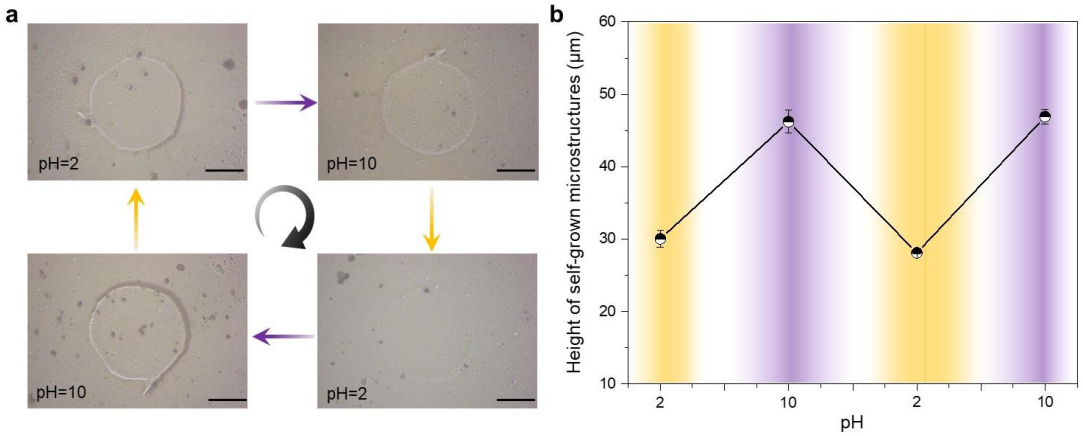

Fig. S19. pH responsive microstructures using AAc (1.0 M, without crosslinker). **a**. Microscope images of the microstructures immersed in solutions with different pH (the buffer solution (pH=2) was 10^{-2} M HCl aqueous solution, the buffer solution (pH=10) was 10^{-4} M NaOH aqueous solution, the temperature was 25 °C). Scale bar, 200 μm. **b**. Height of microstructures changed with pH cycle. Height of microstructures changed with temperature cycle. Error bars represent standard deviation from three replicates.

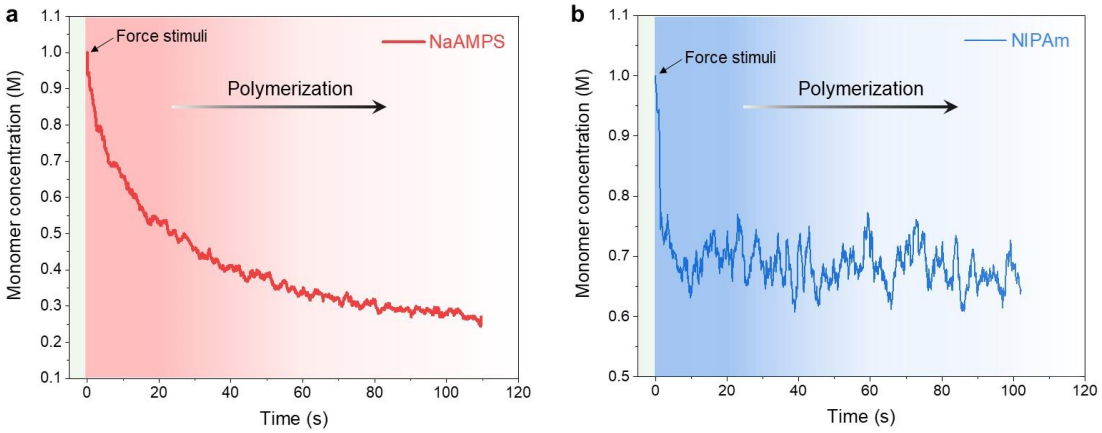

Fig. S20. Kinetics of the force-triggered radical polymerization. The time-resolved near-infrared spectroscopy revealed that the force-triggered radical polymerization almost completed within tens of seconds. **a**. Time-resolved concentration of NaAMPS versus time. **b.** Time-resolved concentration of NIPAm versus time. The initial monomer concentration for NaAMPS and NIPAm was 1.0 M, the temperature was 25 °C. DN hydrogels fed with monomers were stretched beyond yielding point under argon atmosphere, tensile stress was ~0.9 MPa. Here, the curves of time-resolved near-infrared spectroscopy were the average value of at least two replicates.

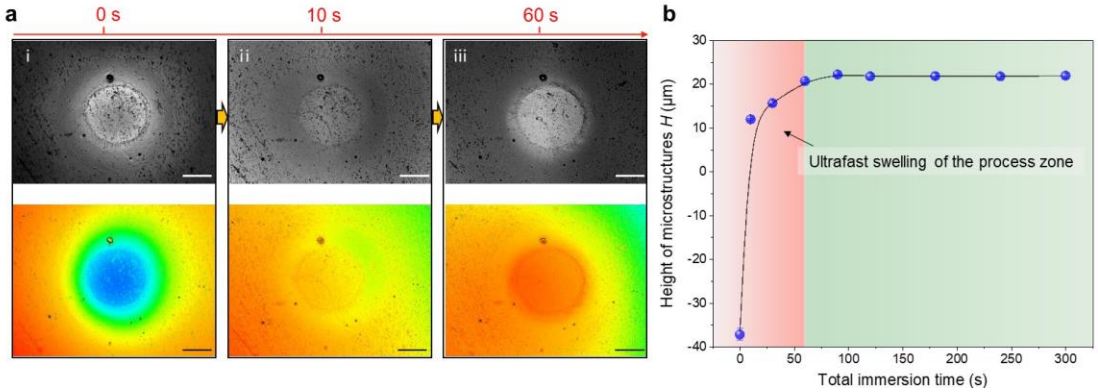

Fig. S21. Observation of the fast swelling on DN hydrogel surface, the process zone was created by regioselective indentation under deionized water without monomer (cylindrical steel indenter diameter was ~568 μm, displacement was ~1000 μm). **a**. The process zone morphology changed over the immersion time. The area of process zone was around ~0.1 mm^2. **b**. Height of reswollen microstructure changed over the immersion time (time scale of equilibrium swelling was approximately 60 s). The height *H* of a DN hydrogel surface for different total immersion times *t* were characterized as follows. First, an indented DN gel surface was observed by the microscope in air (*t* = 0, Fig 21a(i)). The gel was then immersed in water for 10 s, picked up from water and wiped by clean tissues, then observed by the microscope in air (*t* = 10 s, Fig 21a(ii)). Afterwards, the gel was immersed in water for 20 s followed by the microscope observation in the same manner (total immersion time *t* = 10 + 20 = 30 s). Such protocol was repeated several times for this DN hydrogel surface, resulting in *H* as a function of *t* up to 300 s. Error bar represents standard deviation for three replicates. The result indicates that the time scale of equilibrium swelling was about 60 s. Scale bar, 200 μm.

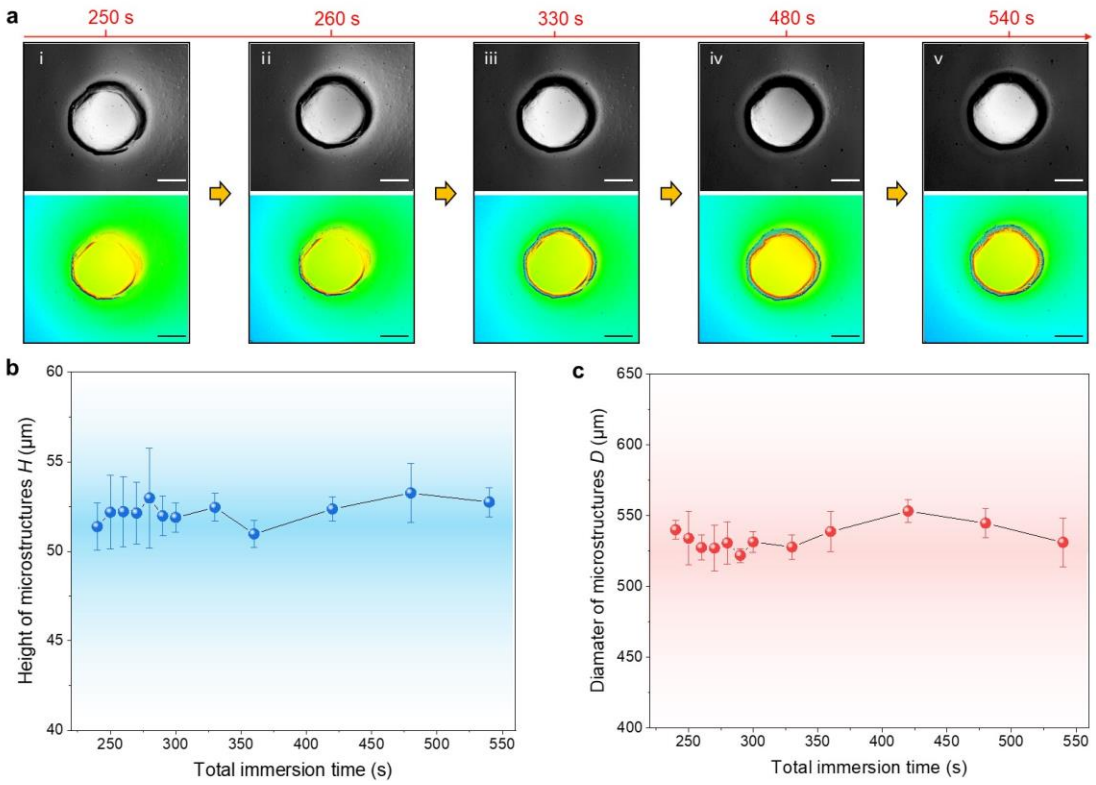

Fig. S22. Evolution of microstructures on DN hydrogel surface in monomer aqueous solution. The microstructures were created by regioselective indentation under NIPAm aqueous solution (cylindrical steel indenter diameter was ~568 μm, displacement was ~1000 μm, indentation speed was 10 mm min^{-1}, the concentration of NIPAm was 1.0 M). **a**. Microstructure morphology changed over immersion time. **b**. Height of microstructures changed over immersion time. **c**. Diameter of microstructures changed over immersion time. The height *H* and diameter *D* of a microstructure on DN hydrogel surface for different total immersion times *t* were characterized as follows. First, a DN hydrogel was indented under the monomer solution in the glove box. The indented gel in the solution was immediately taken out from the glove box, then the gel was observed by the microscope in air after wiping the solution on the gel surface by clean tissues. The time between the end of the indentation and the first microscope observation was 4 min (because of physical distance from the glove box to the microscope), during which the gel was kept in the solution. Hence, we assumed the immersion time *t* of 240 s for the first observation. After the first observation, the gel was immersed again in the solution for 10 s, picked up from solution and wiped by clean tissues, then observed by the microscope in air (total immersion time *t* = 240 +10 = 250 s). Such step of immersion and observation was repeated several times for this DN hydrogel surface, resulting in *H* and *D* as a function of *t* up to 540 s. The results show that the micropatterning was finished before the first observation at *t* = 240 s. Error bar represents standard deviation for three replicates. Scale bar, 200 μm.

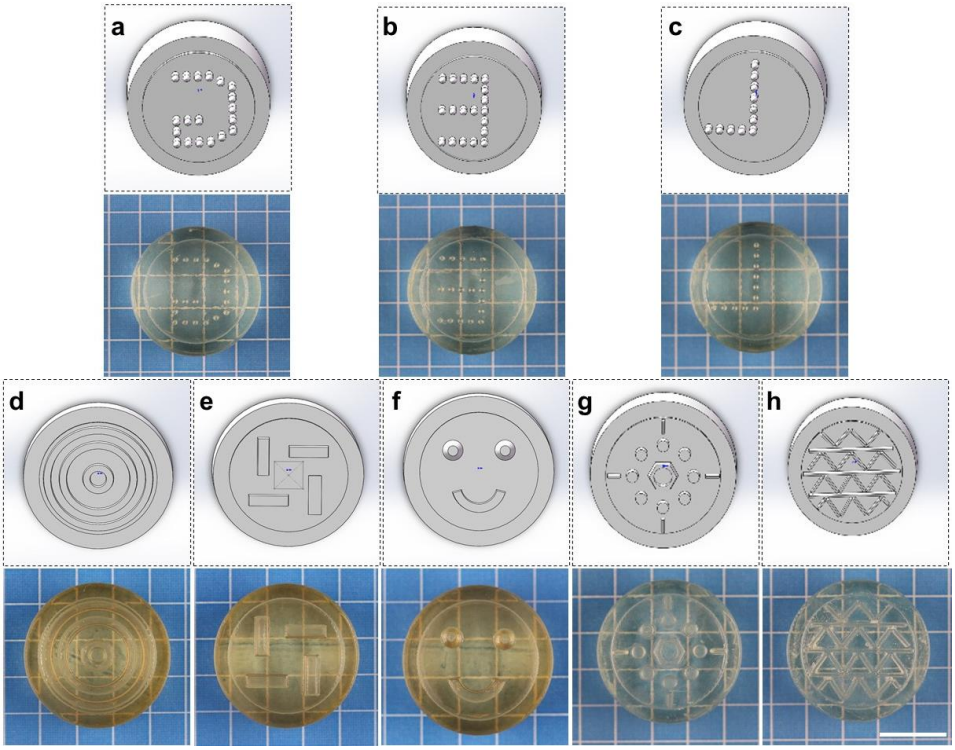

Fig. S23. a-h. Photos of customized models with complex patterns for 3D printing and 3D printed resin indenters. The topographic height of all the 3D printed patterns was ~2 mm. Scale bar, 10 mm.

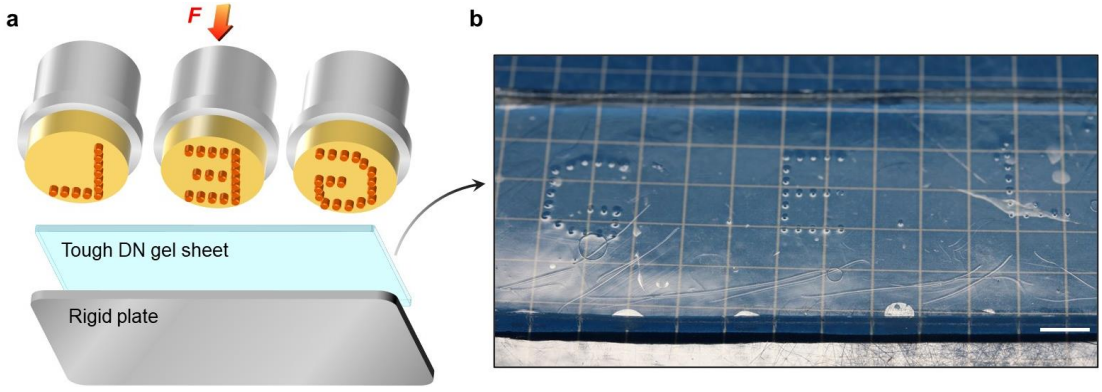

Fig. S24. a. Schematic illustration for programmable micropatterning on DN hydrogel surface. **b**. DN hydrogel surface with the created alphabet of “G E L”. Patterning in NIPAm and MBA aqueous solution (NIPAm concentration was 1.0 M, crosslinker MBA concentration was 5 mol% of the monomer concentration). Scale bar, 5 mm.

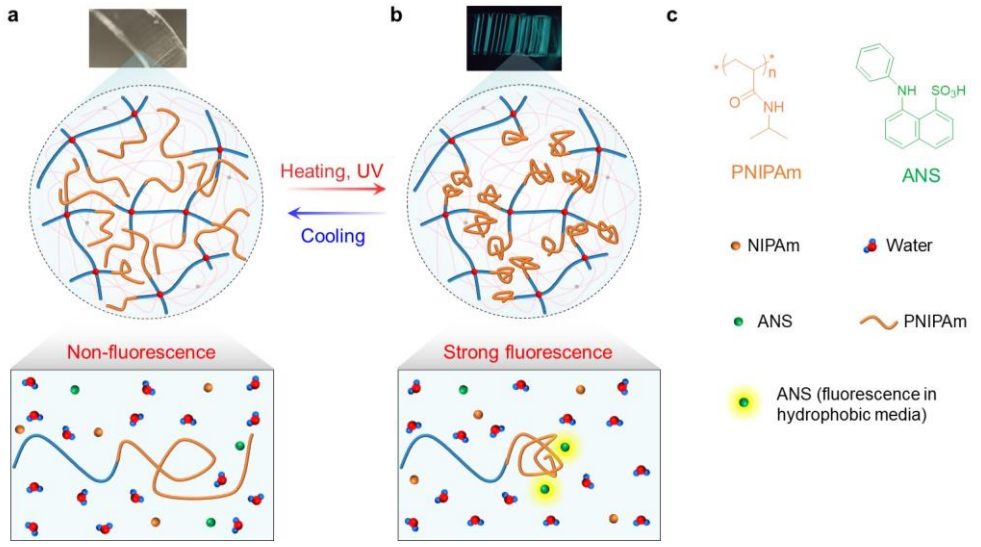

Fig. S25. Molecular mechanism of fluorescence emission from the patterned region on DN hydrogel surfaces[14]. **a**. The patterned region of DN hydrogel hardly exhibits fluorescence at 25 ºC. **b**. The patterned region was visualized when observed at a temperature that exceeds the lower critical solution temperature (LCST) of PNIPAm, because the fluorescent molecule ANS exhibits strong fluorescence only in the hydrophobic environment. **c**. Molecular structures of PNIPAm and ANS.

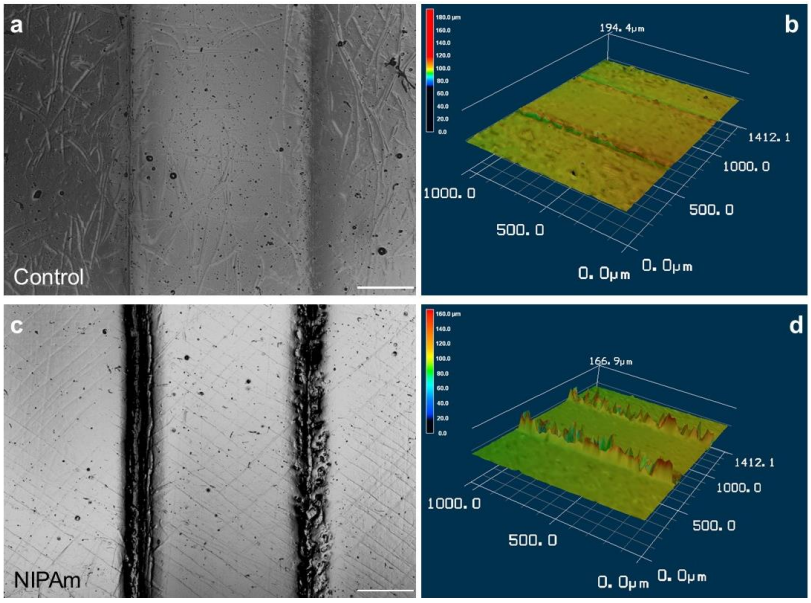

Fig. S26. Surface observation of DN hydrogels with parallel patterns made by a stacked metal blade. Indentation depth was 1.0 mm. **a**. Microscope image of the control sample (damage the hydrogel surface under deionized water), **b**. Three-dimensional topography image of the control sample. **c**. Microscope image of the parallel patterns (damage the hydrogel surface in monomer aqueous solution (NIPAm: 1.0 M), gel surface was washed three times by deionized water prior to the measurements), **d**. Three-dimensional topography image of the parallel patterns. The roughness of the pattern surface R_a was 17.13±2.15 μm, error range represents standard deviation from three replicates. Scale bar, 200 μm.

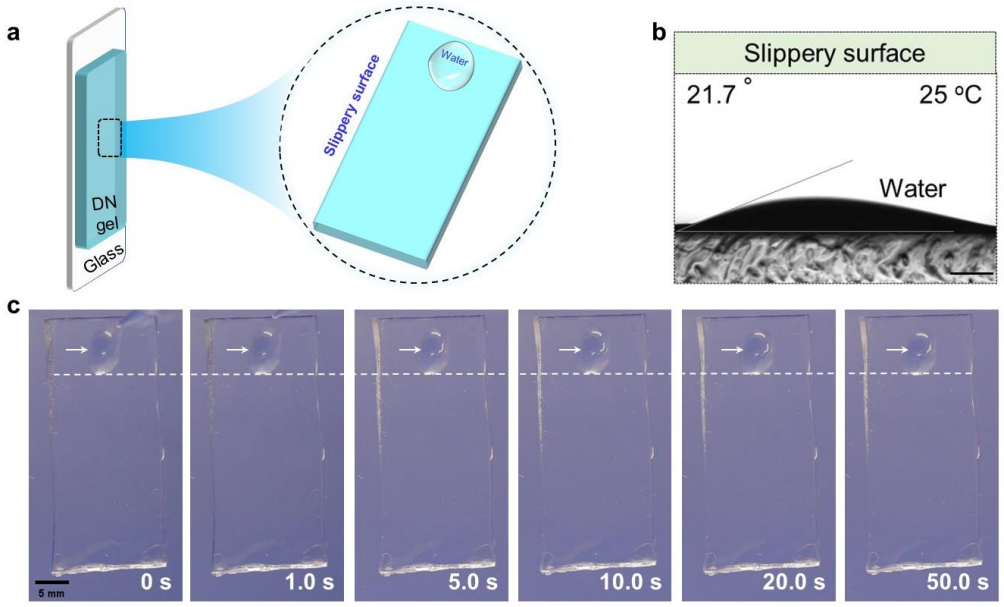

Fig. S27. a. Schematic presentation of a water droplet on smooth hydrogel surface. **b**. Water contact angle of the smooth hydrogel surface. Scale bar, 500 μm. **c**. The state of water droplet on smooth hydrogel surface.

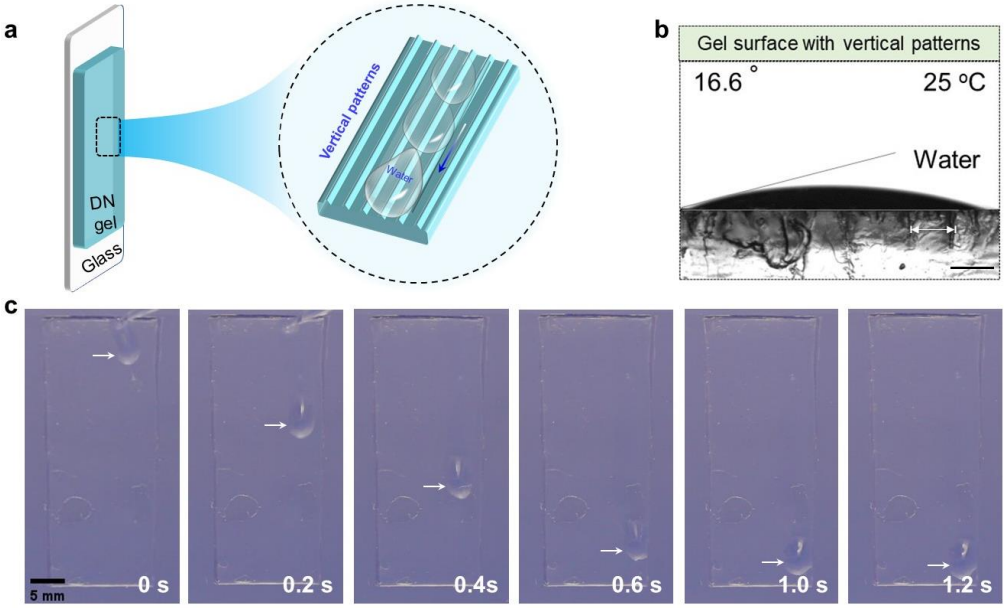

Fig. S28. a. Schematic presentation of a water droplet on DN hydrogel surface with vertical patterns. **b**. Water contact angle on hydrogel surface with vertical patterns. The white arrow indicates the distance (~500 μm) between the two stripes of patterns. Scale bar, 500 μm. **c**. Water droplet fast transport on the patterned hydrogel surface. The patterned gel surface was washed by deionized water three times prior to the measurements.

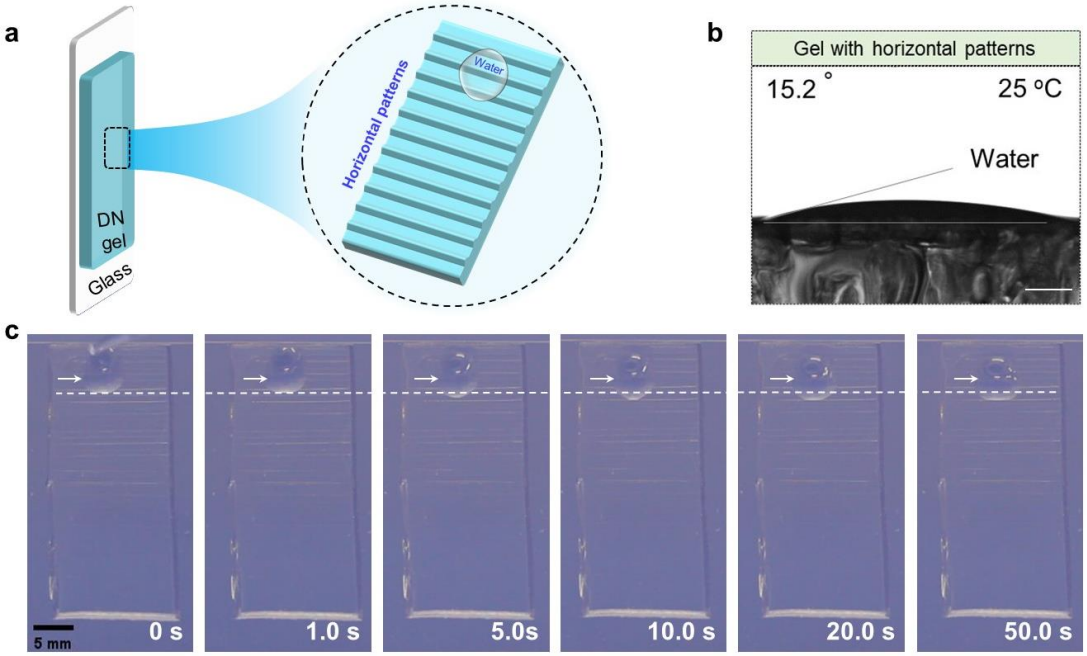

Fig. S29. a. Schematic presentation of a water droplet on DN hydrogel surface with horizontal patterns. **b**. Water contact angle on hydrogel surface with horizontal patterns. Scale bar, 500 μm. **c**. The state of water droplet on the hydrogel surface with horizontal pattern. The patterned gel surface was washed by deionized water three times prior to the measurements.

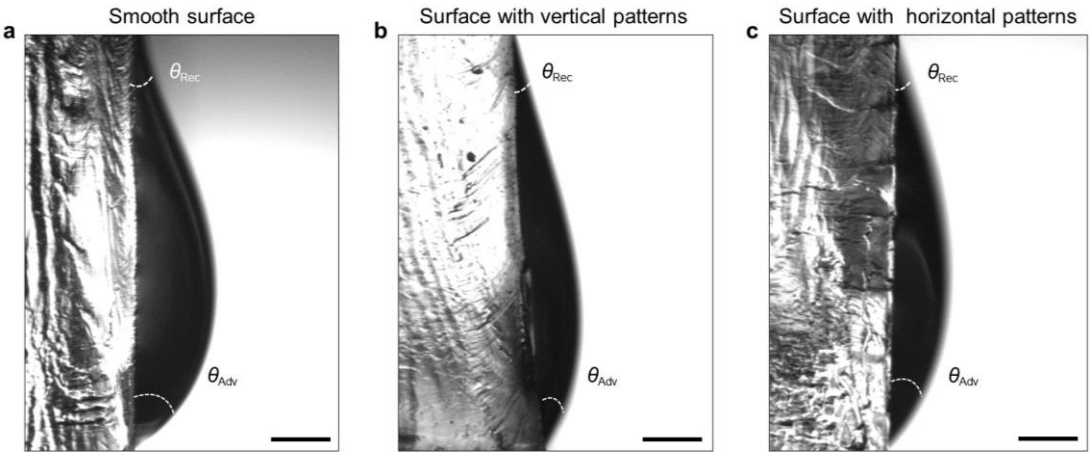

Fig. S30. Contact angle hysteresis and sliding angle of water droplets on different hydrogel surfaces. **a**. Smooth surface (advancing angle is 50º, receding angle is 20º). **b**. Vertical pattern (advancing angle is 30º, receding angle is 15º). **c**. Horizontal pattern (advancing angle is 42º, receding angle is 12º). The advancing and receding angles for the water droplet. Scale bar, 500 μm.

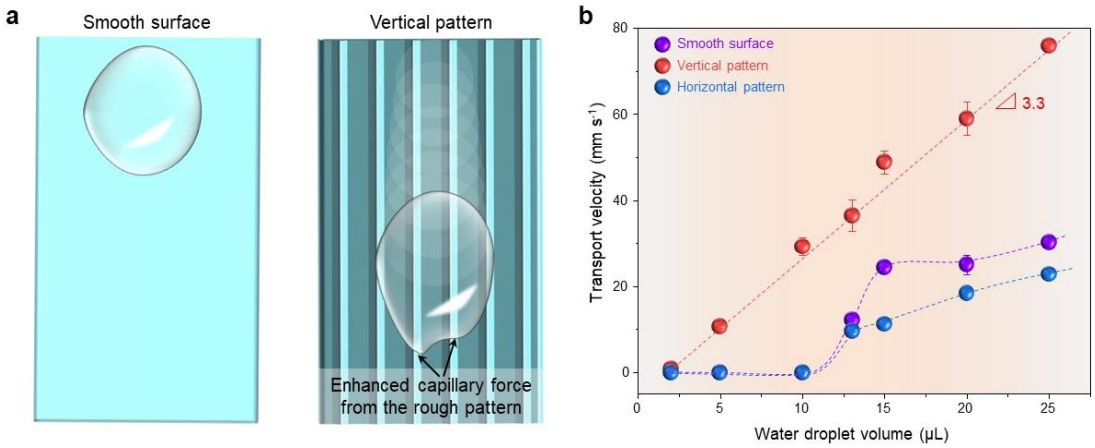

Fig. S31. a, Schematic of water droplet transportation on the smooth hydrogel surface and hydrogel surface with vertical patterns (micropatterning in NIPAm aqueous solution (1.0 M)), the rough pattern was benefit for water wetting and directional transport due to the enhanced capillary force. **b**, Dependence of transport velocity on water droplet volume for different hydrogel surfaces, there was a critical value around 10 μL for smooth surface and horizontal pattern. However, the transport velocity was a linear function of water droplet volume for vertical pattern (Slope, 3.3 mm s^{-1} μL^{-1}).

References

1. Hu, Y. H., Zhao, X. H., Vlassak, J. J. & Suo, Z. G. Using indentation to characterize the poroelasticity of gels. *Appl. Phys. Lett.* **96**, 121904 (2010).
2. Frauenlob, M. et al. Modulation and characterization of the double network hydrogel surface-bulk transition. *Macromolecules* **52**, 6704-6713 (2019).
3. McKee, C. T., Last, J. A., Russell, P. & Murphy, C. J. Indentation versus tensile measurements of Young's modulus for soft biological tissues. *Tissue Eng. Part B Rev*. **17**, 155-164 (2011).
4. Hoshino, K. I., Nakajima, T., Matsuda, T., Sakai, T. & Gong, J. P. Network elasticity of a model hydrogel as a function of swelling ratio: from shrinking to extreme swelling states. *Soft Matter* **14**, 9693-9701 (2018).
5. Sun T L, K. T. et al. Physical hydrogels composed of polyampholytes demonstrate high toughness and viscoelasticity. *Nat. Mater.* **10**, 932-937 (2013).
6. Danielsen, S. P. O. et al. Molecular characterization of polymer networks. *Chem. Rev.* **121**, 5042-5092 (2021).
7. Long, R. & Hui, C. Y. Fracture toughness of hydrogels: measurement and interpretation. *Soft Matter* **12**, 8069-8086 (2016).
8. Bokobza, L. Near infrared spectroscopy. *J. Near Infrared Spectrosc.* **6**, 3-17 (1998).
9. Swinehart, D. The Beer-Lambert law. *J. Chem. Educ.* **39**, 333-335 (1962).
10. Lake, G. J. & Thomas, A. G. The strength of highly elastic materials. *Proc. R. Soc. Lond. A* **300**, 108-119 (1967).
11. Rubinstein, M. *Polymer Physics* Ch. 7 (Oxford Univ. Press, 2003).
12. Matsuda, T. et al. Mechanoresponsive self-growing hydrogels inspired by muscle training. *Science* **363**, 504-508 (2019).
13. Matsuda, T. Study on the self-growing materials in response to mechanical stimuli using double-network system. PhD dissertation (Hokkaido Univ. 2019).
14. Matsuda, T., Kawakami, R., Nakajima, T. & Gong, J. P. Crack tip field of a double-network gel: visualization of covalent bond scission through mechanoradical polymerization. *Macromolecules* **53**, 8787-8795 (2020).